

PROCEEDINGS OF SPIE

[SPIDigitalLibrary.org/conference-proceedings-of-spie](https://spiedigitallibrary.org/conference-proceedings-of-spie)

OASIS architecture: key features

Arenberg, Jonathan, Villareal, Michaela, Yamane, Jud, Yu, Tony, Lazear, Justin, et al.

Jonathan W. Arenberg, Michaela N. Villareal, Jud Yamane, Tony Yu, Justin Lazear, John Pohner, Mitchell Sangalis, Steven L. Jackson, Elisabeth Morse, Ryan Tyler, Pradipto Ghosh, Art Palisoc, Christopher K. Walker, Yuzuru Takashima, Daewook Kim, Siddhartha Sirsi, Aman Chandra, "OASIS architecture: key features," Proc. SPIE 11820, Astronomical Optics: Design, Manufacture, and Test of Space and Ground Systems III, 118200S (24 August 2021); doi: 10.1117/12.2594681

SPIE.

Event: SPIE Optical Engineering + Applications, 2021, San Diego, California, United States

OASIS Architecture: Key Features

Jonathan W. Arenberg^{*a}, Michaela N. Villarreal^a, Jud Yamane^a, Tony Yu^a, Justin Lazear^a, John Pohner^a, Mitch Sangalis^a, Steven L. Jackson^a, Elisabeth Morse^a, Ryan Tyler^a, Pradipto Ghosh^a, Arthur Palisoc^b, Christopher Walker^{c,e}, Yuzuru Takashima^c, Daewook Kim^{c,d,e}, Siddhartha Sirsi^c and Aman Chandra^c

^aNorthrop Grumman Space Systems, One Space Park Drive, Redondo Beach, CA 90278 USA;

^bL'Garde, Inc., 15181 Woodlawn Avenue, Tustin, CA 92780, USA

^cWyant College of Optical Sciences, University of Arizona, 1630 E. University Blvd., Tucson, AZ 85721, USA

^dLarge Binocular Telescope Observatory, University of Arizona 933 N Cherry Avenue, Tucson, AZ 85721, USA

^eDepartment of Astronomy and Steward Observatory, University of Arizona, 933 N. Cherry Ave., Tucson, AZ 85721, USA

ABSTRACT

Orbiting Astronomical Satellite for Investigating Stellar Systems (OASIS) is a mission concept being developed in preparation for the 2021 MidEX Announcement of Opportunity. This paper describes the key features of the OASIS architecture as they are currently understood. OASIS's choice of a large inflatable primary reflector results in large collection areas at very high mass efficiency enabling the science mission. We describe the spacecraft bus, based on Northrop Grumman's LEOstar-2, and the receiver, a heritage design based on the GUSTO balloon heterodyne system. We also discuss the observing strategy and pointing requirements from its planned L1 location. Particular emphasis is placed on challenges to the design, such as momentum management, balancing consumable mass allocations, thermal management, and testing.

Keywords: OASIS mission, system architecture, inflatable optics, lifetime

1. INTRODUCTION

In this paper, we discuss the key architectural features of the OASIS mission. This mission is the subject of a number of papers at this conference and will be a mission concept submitted to the 2021 Astrophysical MidEX announcement of opportunity, expected in final form, later this year.

1.1 OASIS Science Goals

Elsewhere in these proceedings, the scientific objectives and promise of OASIS was introduced and explored. [1]. In mission proposals there is a required element called the science traceability matrix (STM). At the right most column in the STM resides the top level hardware requirements; fundamentally, this is the handoff or interface between the scientists and engineers. In Table 1, we present the driving requirements of that rightmost STM column and show where in this paper (and the others presented) where the interested reader can find our most current results.

Table 1: Science Needs and OASIS Architectural Response

Science Driven Need	Value	Architectural Feature/Design Attribute	Location
Collecting Area	>120 m ²	Large primary (A1), inflatable design	Section 2.1, 2.2 and Refs
Wavelengths	81 to 669 μm	Receiver design	Section 2.3
Mission Lifetime	1 year science mission (after commissioning)	Design for a two consumable system	Section 2.7
Pointing	~2 arcsecond	Two tiered system	Section 2.5
Field Of View	3 arcmin (radius)	Optical Design	Section 2.2 and Refs

2. KEY FEATURES OF THE OASIS ARCHITECTURE

2.1 OASIS Fundamental Challenge

OASIS’s fundamental challenge is the large collecting area, >120 m². Without regard to cost or schedule limitations implicit in a MidEx Mission, consider Figure 1: this is a plot of the finished (polished) optical area versus total flight system mass, for several flight programs and some well-studied missions. The dotted line is a linear fit to the set of JWST, Chandra and the LUVOIRs, which can be characterized as a segmented system, has a slope of approximately 300 kg/m². If OASIS were to select a system based on this class of architecture, for a mass cap of 1700 kg, enabling both MidEx launch options, the maximum collecting area would be 1700 kg/300 kg/m² or 5.6 m² which is about a 1.4 m radius primary, clearly not sufficient for OASIS’s requirements.

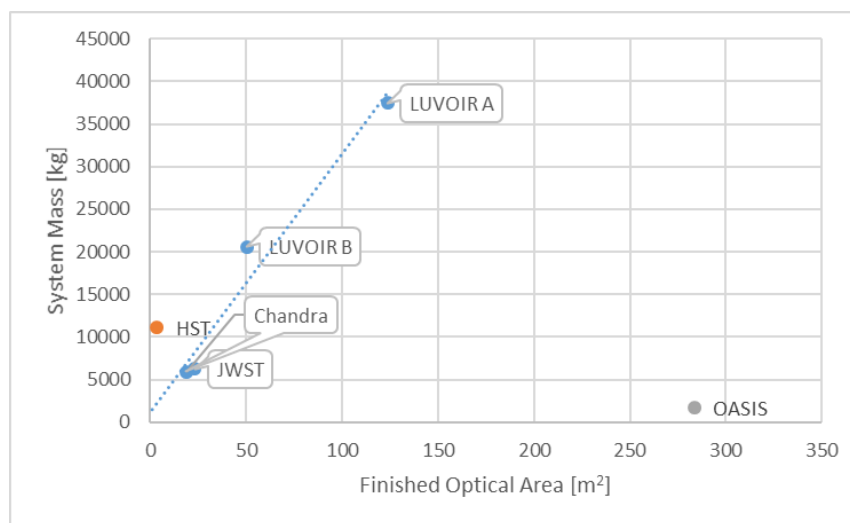


Figure 1. System mass of telescopes as a function of their finished optical areas. A traditional telescope design under the MIDEX mass cap would have a maximum collecting area of ~5.6 m². OASIS’ inflatable design will have a primary mirror area of ~280 m² at a vastly lower system mass than previous traditional designs.

To make OASIS a reality, a vastly more mass efficient system architecture is required, one approximately 20 times more efficient or roughly 13 kg/m² at the systems level. Fortunately, for our present application such an architecture has been explored and examined, specifically inflatable optical systems. Inflatable systems have been part of the aerospace milieu

since 1960, with Project Echo [2], and other early experiments. [3] There are also many examples of inflatable systems being considered as the basis of space based optical systems. [4,5,6,7,8,9] To underscore the idea that inflatable optical systems are hardly a novel concept, consider the results of a literature search for inflatable reflectors and antennas for space, shown in Figure 2. Figure 2 shows that this basic architecture has been investigated over the past four decades. Reported activity and technical development of inflatable membrane telescopes peaked around the year 2000, largely under US government funding. Following the peak a lull has existed until our current efforts which if included in Figure 2, would be off scale. Interest in an inflatable design for space based applications and OASIS in particular should be seen as a revival and able to build on significant development work. A NASA experiment in the late 1990's, the Inflatable Antenna Experiment, a 14 m diameter parabolic reflector deployed from the space shuttle on Mission STS-77 provides direct legacy to OASIS. [10]

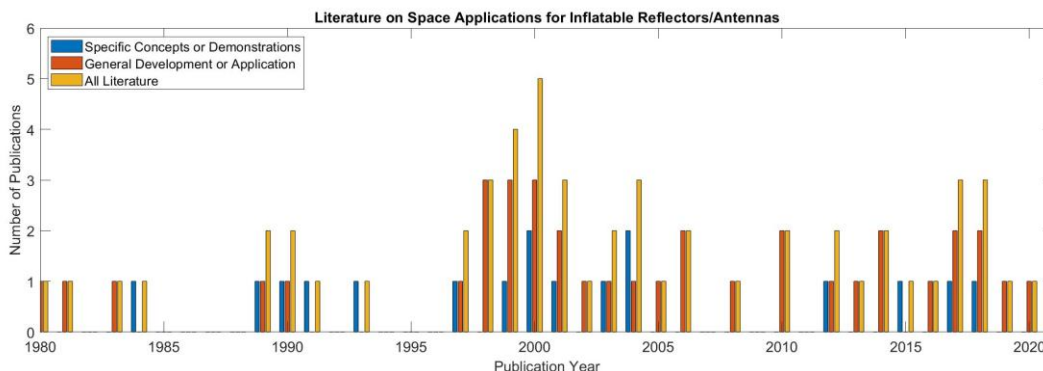


Figure 2. Literature on Inflatable Space Telescopes from the past 40 years.

To show the viability of OASIS as a mission concept, we have tried to address many of what are the “obvious” questions. Some of the questions are not only obvious, but are complex and the answers lengthy. Our current understanding of the impact of the environment on the ability to keep the primary reflector inflated is an entire separate report. [12] The modeling and process of modeling an inflatable optic and the resulting optical design are separate reports. [13][14] Key to program success is the ability to verify aperture stability. For a system as large as OASIS, we need to show that it is possible to measure the primary aperture and to do so without system verification in a vacuum chamber. [15] OASIS is a large system and a reader will correctly ask about momentum management, which is addressed in this paper in Section 2.6. Another reasonable questions is, “what runs out first, propellant or inflatant?” This question is the subject of Section 2.7.

2.2 Top Level Architecture

OASIS consists of the inflatable primary, referred to as A1, connected to the spacecraft by 3 booms, shown in Figure 3. The light from the primary is reflected in to the corrector module, which has tilt/tils mirrors for image stabilization and adjustable mirrors for wavefront correction. [13]

The inflatable itself is constructed from ½ mil, 6.7 μm thick polyimide film. This thin film allows OASIS to reach the critical film strain with low pressures. [14] There are two main options for realizing an inflated optic. The first is for two flat plates and a stiff perimeter interface and is called a Hencky reflector after the first person to solve the mechanical problem and determine the shape of the inflated membrane. [16] The second is a shaped parabolic reflector.[14] OASIS will be a shaped parabolic reflector, we have made this selection for several reasons:

- The operating pressure for a Hencky reflector is 18 Pa and for a parabola 3.5 Pa. This pressure difference results in a large difference in required make up gas mass. The Hencky reflector architecture requires 18/3.5~7 times more gas mass to keep it inflated over its lifetime. [12]
- The Hencky reflector requires very large optics in the corrector module. The secondary reflector would need to be ~2.4 m diameter in this case. For the parabola that secondary reflector is ~0.5 m diameter. This is a clear driver for mass, cost and schedule.

It is for these reasons that OASIS is baselining a shaped parabolic reflector. Figure 4 shows the solution space for the combinations of telescope diameter and radius of curvature which can meet the science requirements for each band. The basis for the design plot is discussed in detail in a companion paper. [11] One such solution is a 17 m diameter primary with a radius of curvature of 50 m.

Figure 3 shows a rendering of the parabolic telescope once deployed. The primary reflector will be supported by three rigidizable booms and a rigidized torus which provides the mechanical interface between A1 and the boom. It is expected that the deployment accuracy of the booms will be of order of a few 0.001 inch. This is too large to be accommodated passively, so all three booms will have low duty cycle mechanisms to adjust their position and will provide control of the despace and tilt of A1.

The ability of OASIS to meet its science requirements is directly dependent on its ability to maintain the reflector shape during observations. To ensure this, OASIS will be equipped with a pressure control system (PCS). The largest obstacle to pressure maintenance is gas loss from micrometeoroid punctures. We therefore heavily focus on how the inflatant will be lost with time to ensure enough mass is budgeted to meet the mission lifetime requirement. [12]

Even when maintained at ideal conditions, the A1 shape will not be perfect. Corrections will be needed, which can be accommodated by strategic placement of secondary optics [11]. Tests will be conducted on A1 following its manufacture. The as built shape will be used to calculate the on-orbit shape of A1 and correct some of the errors by altering the prescriptions of the second and third powered optical surfaces, A2 and A3. [13][15]

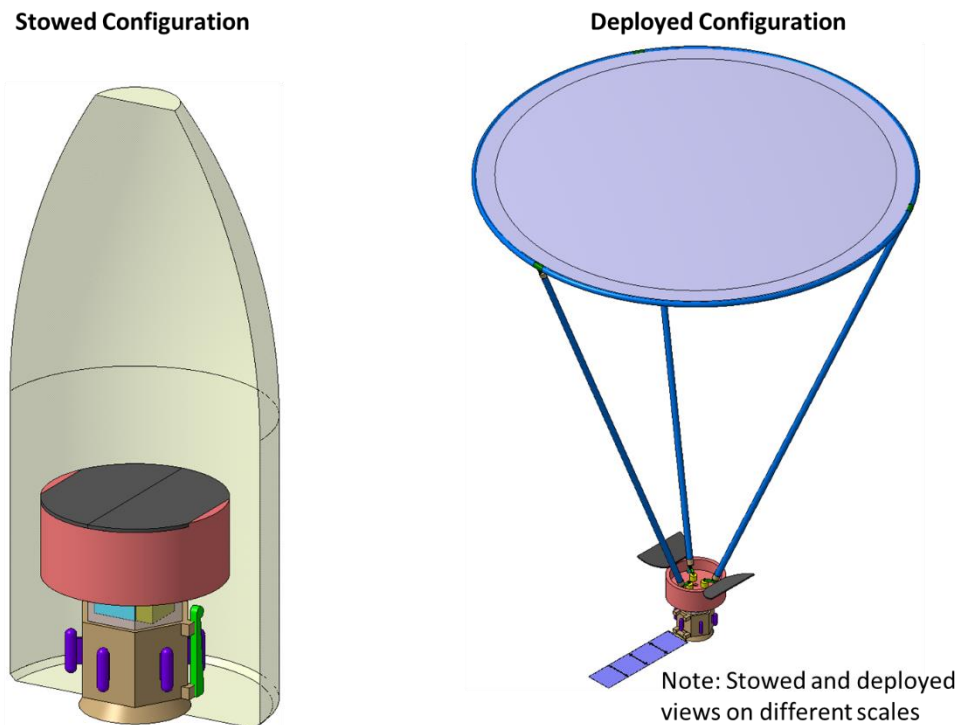


Figure 3. Schematics of stowed (left) and deployed (right) configurations for OASIS.

The OASIS spacecraft design is derived from Northrop Grumman's flight-proven LEOStar-2 product line. Currently operating Explorer-class missions with a LEOStar-2 spacecraft include the Ionospheric Connection Explorer (ICON, launched 2019), the Transiting Exoplanet Survey Satellite (TESS, launched 2018), and the Orbiting Carbon Observatory-2 (OCO-2, launched 2014), among others.

The spacecraft uses a cost-efficient single string design with selective redundancy and is capable of meeting the mission requirements with robust margin. Features of the spacecraft subsystems include:

- The bus structure is a hexagonal Aluminum honeycomb design flown on previous Explorer class missions.

- The propulsion subsystem leverages flight-proven components to implement the monopropellant hydrazine propulsion system. The on-board propulsion system is responsible for carrying out maneuvers to reach the science orbit, to maintain the science orbit (i.e. station keeping), and to de-saturate the reaction wheels. The delta V requirements for OASIS are quite modest and within the envelope of previous missions.
- The thermal control subsystem uses a cold-bias passive design with radiative cooling and heaters. The design is simplified by the orbit geometry and pointing strategy: there is no eclipse in the science orbit, the spacecraft body remains illuminated by sunlight (i.e. not shadowed by the reflector), and the body panels will have consistent fields of view (deep space versus sunlight) for all observation targets.
- The power subsystem uses a shunt-regulated Direct Energy Transfer (DET) system with one single-axis articulated solar array (SA) wing, a Li-Ion battery system, and power control electronics housed in the primary avionics unit together with the command and data handling electronics.
- The attitude control subsystem meets pointing precision and accuracy requirements with the use of a standard 4-wheel pyramid configuration reaction wheel assembly, two orthogonal star tracker optical heads, and an inertial reference unit.
- The telecom subsystem uses a simple all S-band system with two hemispherical quadrifilar low gain antennas (LGAs) coupled via a 3-dB hybrid, as flown on all LEOStar-2, achieving an omni-directional antenna pattern for low bandwidth command and telemetry. A body-fixed High Gain Antenna (HGA) is used to downlink science data via the Deep Space Network. The range of Sun-Earth angles throughout the L1 orbit inform the HGA mount angle to ensure the solar array is not shadowed by the reflector when pointed towards Earth, see Figure 7.
- The command and data handling (C&DH) subsystem is housed in the same primary avionics unit that contains the power subsystem electronics. The unit includes a RAD750 microprocessor which hosts the flight software responsible for attitude control functions, command and data handling functions, and power and thermal control functions. The C&DH subsystem provides the command and telemetry interface to the instrument electronics, and receives science data from the instrument for non-volatile memory storage via a separate high bandwidth link.

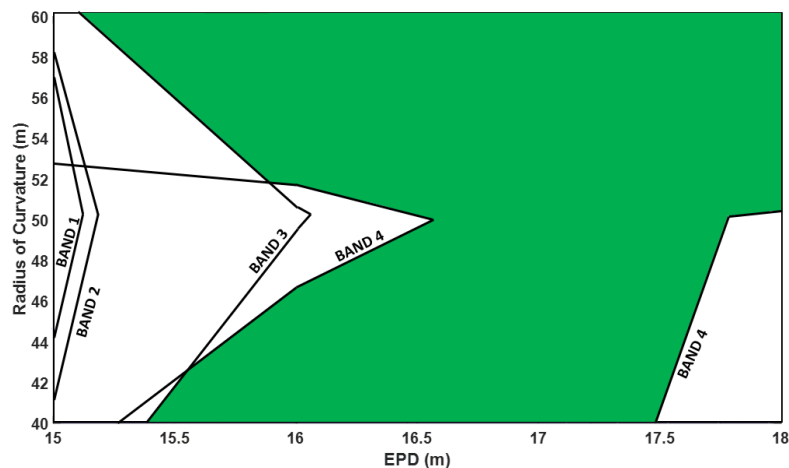


Figure 4. Combinations of Entrance Pupil Diameter (EPD) and radius of curvature which can satisfy hypothetical effective area requirement for each band.

2.3 Receiver

In order to meet the science objectives described in the OASIS Science Traceability Matrix (STM), OASIS will have a cryogenic superheterodyne receiver system with 4 frequency bands ranging from 455 GHz (660 μm) to 3692 GHz (81.2 μm). The receiver architecture is shown in Figure 5.

The Band 4 receiver (like Band 3 and 4) is a single-polarization system using a hot-electron bolometer (HEB) mixer configured for double-side band (DSB) operation. However, due to its high frequency (~3.7THz), it utilizes a quantum cascade laser (QCL) as the LO. It has a receiver noise temperature of ~700 K. The Band 3 output feeds an ACS with 3.7 GHz of IF bandwidth and 5.37 MHz of spectral resolution. The Band 4 mixer can be tuned over ~10 GHz by adjusting the DC bias and operating temperature of its QCL. Band 4 has a diffraction-limited beam spot size of 2.3 arcsec.

The OASIS receiver system employs a total of 9 backend spectrometers; six for Band 1 and one spectrometer each for Bands 2-4. Each spectrometer contains 1024 channels with 14 bit word sizes, yielding a receiver science data rate of ~130 kbps.

2.4 Orbit

The current orbit selection for OASIS is a halo orbit around the Sun-Earth first Lagrange point, denoted SE L1 or L1. This orbit is eclipse free and provides a vantage point to not only galaxies, protoplanetary disks, planets, moons and comets but the Earth and Moon as well.

A sketch of the orbit in an L1 centered coordinate system is shown in Figure 6. To keep the solar array illuminated, OASIS must be pointed at least 17° from the anti-solar or X direction. In order to communicate and transmit data to the ground, OASIS must point at Earth. Note that the science program also calls for Earth observations. Furthermore, OASIS must be able to point at the Moon.

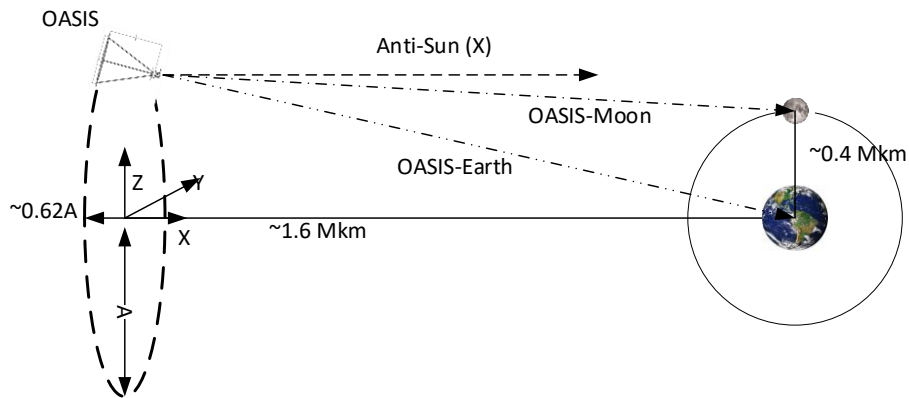


Figure 6: Sketch of the geometry of OASIS's Sun-Earth L1 halo orbit. (Note: drawing is not to scale)

A halo orbit is typically described in the so-called synodic reference frame, which is a Cartesian system centered on the barycenter of the primary bodies (the Sun and the Earth-Moon system in this case), as schematically illustrated in Fig. 6. In this coordinate system, Earth lies on the X axis, 1.6×10^6 km in the positive or anti-sunward direction. The Moon's orbit is represented as a circle of radius 400,000 km in the X-Z plane. Under a purely three-body point-mass gravitational model, which is appropriate for initial orbit design, the halo orbit is approximately modeled as an ellipse in the Y-Z plane, the major axis is in the Z direction and the minor axis in the Y direction. In terms of in-plane and out-of-plane motion amplitudes, a halo orbit may be expressed as [16]:

$$x = -kA_x \cos(\lambda t + \phi)$$

$$y = A_y \sin(\lambda t + \phi)$$

$$z = A_z \sin(\nu t + \psi)$$

The proportions of this orbit are approximately 8 to 5, ($A_z:A_y = 8:5$), or the minor axis is ~0.62 of the major axis. The period of this orbit is 6 months. Using this geometry the angle from the anti-sunward direction of the Earth and the Moon can be calculated for a 455 day period (90 days commissioning and a 1 year science mission). The sun-angles can be plotted as a function of time and the size of A. For $A=800,000$ km (497,097 miles), Earth always meets the criterion of being 17° or greater from the anti-sun direction. Earth's visibility is shown in Figure 7. Figure 7 also indicates that the Moon is also visible to OASIS about 72% of the time.

Figure 8 shows the simulated transfer trajectory (in yellow) of a representative Earth-to-L1 mission, and the corresponding mission halo orbit (in blue), projected on the XY plane of the synodic frame, while Figure 9 depicts the 3-D view.

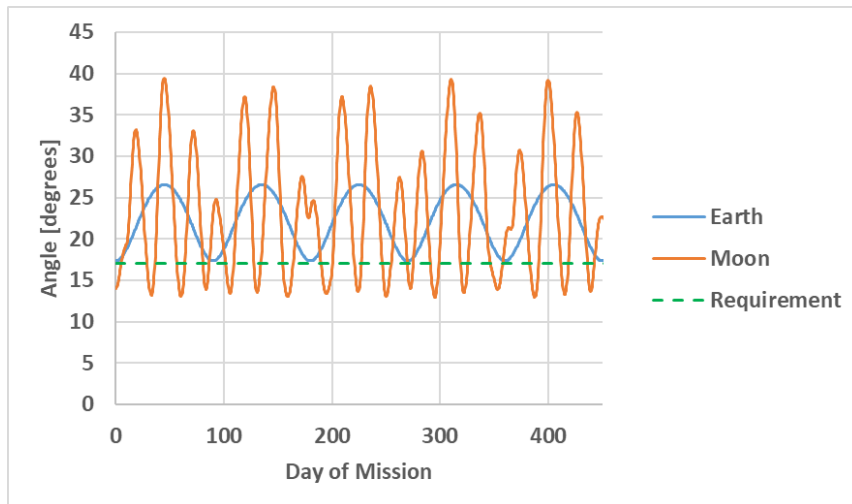


Figure 7. Time series of the angle between the Earth's and Moon's location and the anti-solar direction. The architecture requires that OASIS must point at angles greater than 17 degrees from the anti-solar direction. This figure shows that the Earth and moon will be in OASIS's field of view for the majority of the mission.

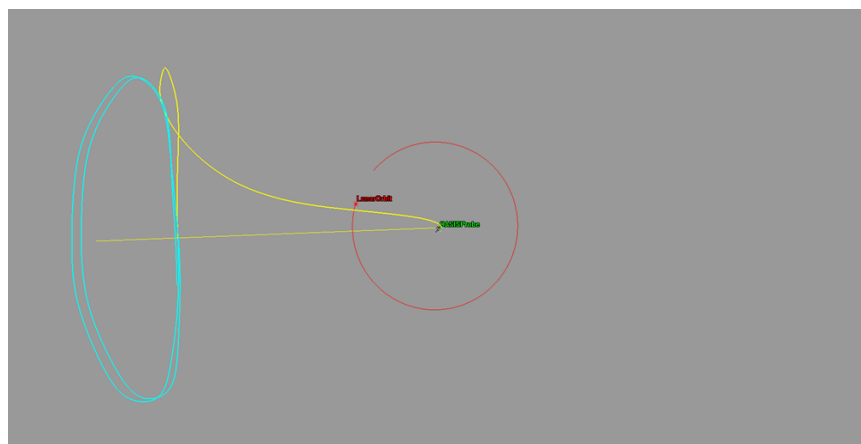


Figure 8. A typical L1 halo orbit and Earth-to-L1 transfer trajectory, XY projection

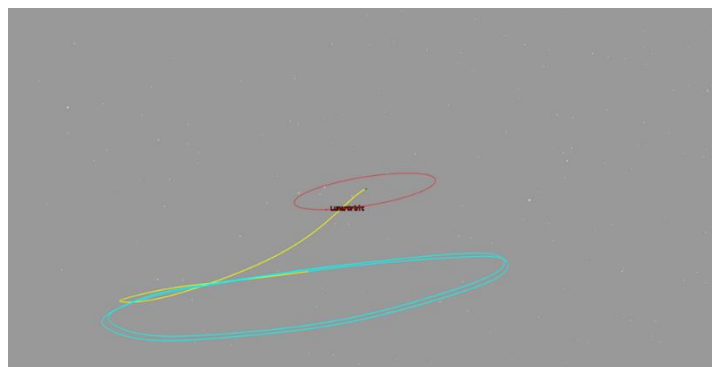


Figure 9. A typical L1 halo orbit and Earth-to-L1 transfer trajectory, 3-D view.

2.5 Observations

The OASIS science objectives and observatory architecture drive the observing strategy. Measurement of the hydrogen-deuterium (HD) spectral line with OASIS band 3 sets typical observation periods on the order of 12 hours, when using standard best-practice observational techniques such as position-switching and on-the-fly-mapping. These techniques require agile repositioning of the beam on the sky. Since spectral lines within bands 1 and 2 are brighter than HD in band 3, bands 1 and 2 will be spectrally swept to collect a number of lines over the observation period. All four observing bands will be collected simultaneously. With only a single pixel, the observatory is capable of observing only a single target at a time; in order to address a new target, the observatory must repoint to the new target. Figure 10 illustrates the relative movement of the observatory as it migrates from one target to another using a preliminary list of targets. In order to meet its science objectives, OASIS must observe galaxies, protoplanetary disks, and solar system objects including the Earth, the Moon, planetary bodies further from the Sun than Earth, and comets; therefore OASIS must have a nearly full-sky field of regard.

The OASIS architecture constrains the observing strategy. In order to keep the OASIS A1 primary reflector from eclipsing the solar arrays, the observatory may not point within 17 degrees of anti-solar. The angular momentum management strategy (see Section 2.6) and thermal distortions of A1 favor pointing as close to anti-solar as possible. These constraints put a sweet spot in the 17 degree to 60 degree off-anti-solar range, with capability out to 90 degrees off-anti-solar. Combined with the ~ 1 degree/day rotation of the sky from OASIS's orbit at L1, the observatory will be capable of addressing all of its targets over the course of a year.

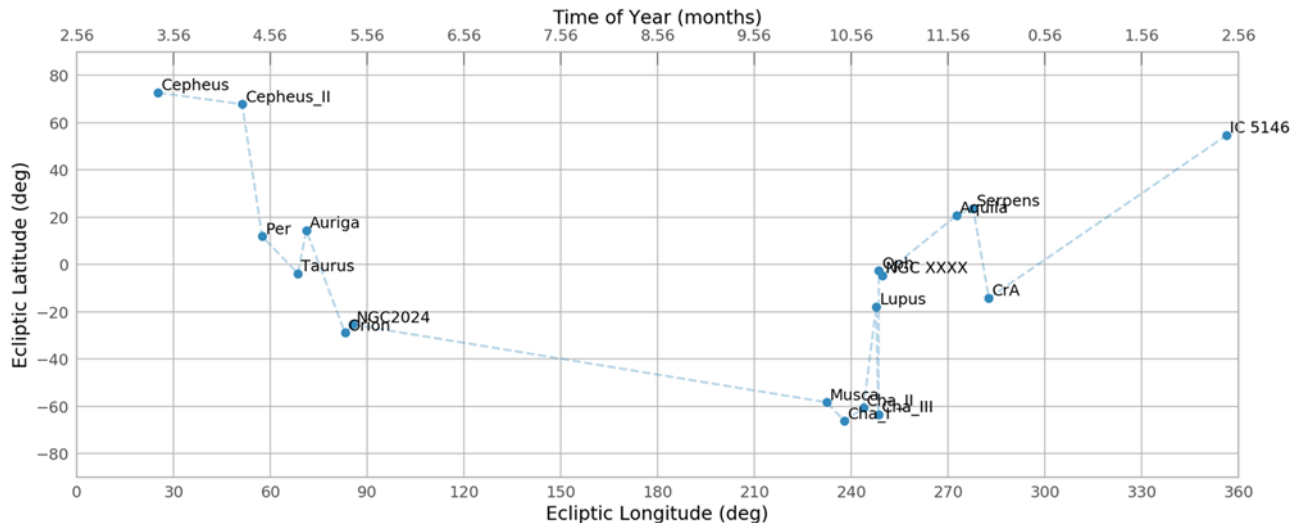


Figure 10. Preliminary targets and their respective longitude and latitudes at the time of observation. Note: this is a very early version of the target list, with many targets missing (particularly between 120-210 longitude).

OASIS will minimize the variety of thermal environments by preferentially rotating about an axis parallel to the solar array axis, called the “pitch” axis. Since angular momentum builds up about the off-anti-solar axis, keeping this axis consistent also allows optimization of the guidance, navigation and control system (GNC). Additionally, this will provide a consistent set of spacecraft faces that will never be illuminated by the sun and consistent geometry of OASIS relative to the Earth. OASIS will be capable of unloading its accumulated angular momentum during the 12-hour observational period if necessary. Additional details of the angular momentum management are discussed in Section 2.6.

Observing targets are sequenced by minimizing their off-anti-solar angle. By waiting for the Earth-Sun line to align with the target's ecliptic longitude, this off-anti-solar angle is minimized and equal to the ecliptic latitude. Targets with ecliptic latitudes between -17 degrees and +17 degrees will be observed before or after their off-anti-solar angle minimum to maintain the 17 degree off-anti-solar keep out.

A typical observing sequence of a single target using position-switching is as follows. The target is positioned within the beam by first slewing the observatory using the GNC System to within 1 arcmin, allowing the observatory structural transients to settle, then to within 0.5 arcsec using the Steering Mirror System (SMS) with a peak-finding spiral scan.

Photons from the target (ON) are collected for 20 seconds; the 20 second period is set by the receiver Allan time the time period for which a frequency is stable. During the ON integration, the bolometer channel (BOLO) is fed back into the SMS to provide active control of the beam positioning on the peak. Then the receiver's flip mirror's position will toggle, allowing the detectors to view the integrated calibration blackbody load (CAL) held at 100 K for 5 seconds. The flip mirror will actuate to put the beam back on the sky and two additional ON/CAL measurements will be made, for a total of 3 ON and 3 CAL measurements. In order to mitigate systematic uncertainties, the SMS repositions the beam to between 10 arcsec and 60 arcsec (depending on target type) off the target and collects 20 seconds of data (OFF). If appropriate, the band 1 or band 2 local oscillators (LOs) will re-tune to target a new spectral line. The SMS will then reposition the beam on target, and this 95-second long ON/CAL/ON/CAL/ON/CAL/OFF/LO sequence repeats for the 12-hour observation duration.

If the angular momentum saturates during the 12-hour period, this process is interrupted while the angular momentum is unloaded. The beam is recentered on the target with an observatory slew, the transients allowed to settle, and a spiral steering mirror scan. Following this, the observing sequencing is resumed from where it was interrupted.

OASIS will also observe some non-sidereal targets with expected apparent angular velocities of <0.3 arcsec/sec. A series of quaternions of the expected target position is input into the GNC system, and then the observation is treated as described previously. The very low apparent angular velocity means the angular position and therefore observatory condition does not significantly change over the course of the observation. The observatory's high moment of inertia stabilizes the rotation.

An on-orbit commissioning period will observe standard reference objects and characterize observatory parameters. Measurements of the Earth's limb or the Moon's limb will characterize the beam shape and SMS response. The planets or reference stars like Vega will characterize the receiver sensitivity. Any known point source will characterize the pointing offset between star tracker and science beam, and structural transients. Observations of deep space will characterize the receiver stability.

With this observation strategy, OASIS will have a total integration efficiency of $>90\%$, observe all of OASIS's science targets over the course of 1 year, and satisfy the OASIS architectural constraints. Although a year's worth of sky rotation is required to observe targets across the entire sky, the threshold science objectives may be satisfied with an observing efficiency as low as 25% over the course of 6 months, indicating OASIS has significant margin in its observing strategy.

2.6 Momentum

As discussed in Section 2.5, OASIS must observe targets at off-anti-solar angles typically between 17 and 60 degrees and as high as 90 degrees for typical periods of 12 hours. The solar radiation pressure on the large primary reflector A1 generates a significant amount of torque on the observatory and presents an angular momentum management challenge. Further, the torque on the observatory is such that pointing the observatory boresight anti-solar is an unstable equilibrium: rotating the observatory about one axis results in a torque that drives increasing rotation about that same axis. This section describes considerations for management of OASIS's angular momentum and demonstrates that it can be successfully managed over the life of the mission.

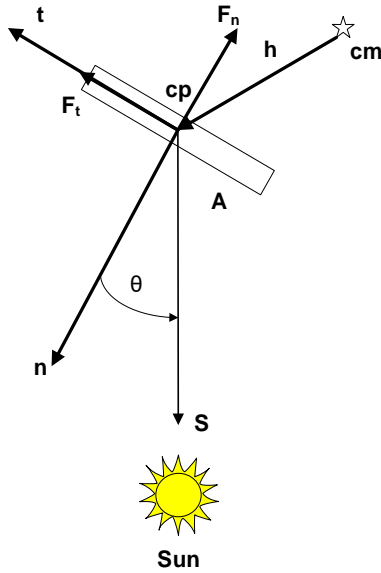


Figure 11. Solar radiation force components

The solar radiation pressure (SRP) on a large spherical cap, representing A1, and the resulting torque on a simplified observatory system model has been modeled. The geometry is shown in Figure 11 and produces normal and transverse forces

$$F_n = -AP_s \cos \theta \left[(1 + C_s) \cos \theta + \frac{2}{3} C_d + 0.63 C_a \right]$$

$$F_t = AP_s [1 - C_s] \cos \theta \sin \theta$$

which then produces a torque of

$$\boldsymbol{\tau} = \mathbf{h} \times (F_t \mathbf{t} + F_n \mathbf{n})$$

Where $C_s + C_d + C_a = 1$ are the specular reflection, diffuse reflection, and absorption coefficients and \mathbf{n} and \mathbf{t} are the unit normal and unit tangent vectors. Locations “cp” and “cm” are the center of pressure and center of mass. The optical properties for A1 are given in Section 2.7, Thermal. The resulting torque is shown in Figure 12 where the y-axis corresponds to the pitch axis (i.e. the same axis as the off-anti-solar angle), the x-axis corresponds to roll about the boresight, and the z-axis corresponds to observatory yaw.

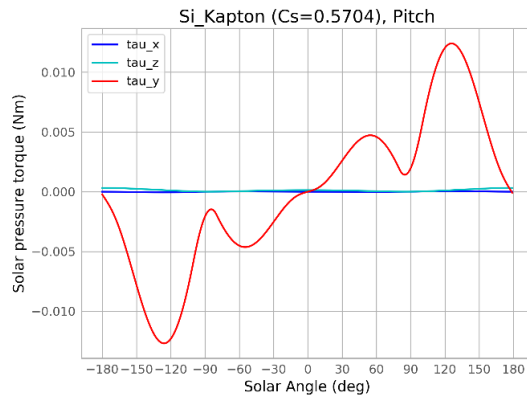


Figure 12. Solar radiation pressure as a function of the solar angle.

Since OASIS must hold its attitude for periods of 12 hours, this torque will accumulate into angular momentum that must be absorbed by the observatory reaction wheels. In order to simplify the design, the dominant rotation axis is kept

consistent in the observatory body frame and called the “pitch” axis. To address different targets, the observatory will rotate about its boresight to make the target reachable with a pitch rotation. Further, since OASIS must avoid pointing within 17 degrees of anti-solar to ensure the solar arrays stay illuminated, only positive off-anti-solar angles greater than 17 degrees are used. Thus, the observatory maintains a pitch angle between 17 and 90 degrees at all times, with only small yaw angles ($|\text{yaw}| < 5$ degrees). This ensures angular momentum builds up only in the pitch direction.

The angular momentum is managed using two mechanisms: with a Reaction Wheel Assembly (RWA) and with thrusters in the Propulsion Subsystem (PSS). The RWA is a typical symmetric 4-wheel pyramid configuration with per-axis capacity around 200 Nms and per-axis torque around 0.2 Nm. The RWA torque capacity is more than an order of magnitude larger than the maximum expected solar torque, therefore an unsaturated RWA will be able to maintain strong control over the observatory attitude. Typical thruster pairs using a specific impulse consistent with end-of-life performance of 150 s are mounted to the spacecraft. The thrusters are responsible for unloading the angular momentum stored in the RWA once a specific threshold is reached. Observations will be performed during periods where the RWA is maintaining the attitude; although it may be possible to make meaningful observations during the thruster unloading period, the system model assumes this is not the case.

The angular momentum capacity of the RWAs is allocated according to Table 2. Half of the allocation is held as margin in this early stage of development to provide high flexibility as the design progresses. 20 Nms (10%) is reserved for slewing the observatory. This corresponds to a maximum angular speed of about 2 arcmin/s, or 2 degrees/minute. Including the angular acceleration, the observatory can slew 10 degrees in about 7.5 minutes.

Table 2. Allocation of angular momentum capacity of the Reaction Wheel Assembly.

Component	Allocation %	Allocation Value (Nms)
Margin	50%	100
Maneuvering & Tracking	10%	20
Point-of-No-Return Reservation	0.5x %	$x(\theta)$, depending on off-anti-solar angle
SRP Accumulation	40 – 0.5x %	$80 - x(\theta)$
Total	100 %	200 Nms

Since the SRP torque pushes the observatory to ever-increasing pitch angles, a minimum amount of angular momentum is required to restore the attitude to a low-SRP torque state at around 17 degrees off-anti-solar. This minimum Point-of-No-Return (PoNR) Reservation increases as the off-anti-solar angle θ increases. Depending on the off-anti-solar angle of the target, this PoNR angular momentum is reserved.

Whatever angular momentum capacity available after margin, maneuvering, and PoNR is taken out is used to accumulate the solar radiation pressure torque. This has been used to estimate how long OASIS may observe a target before the RWAs saturate and must be unloaded, and is shown in Figure 13. OASIS will be able to point at its target for many hours for all of its targets.

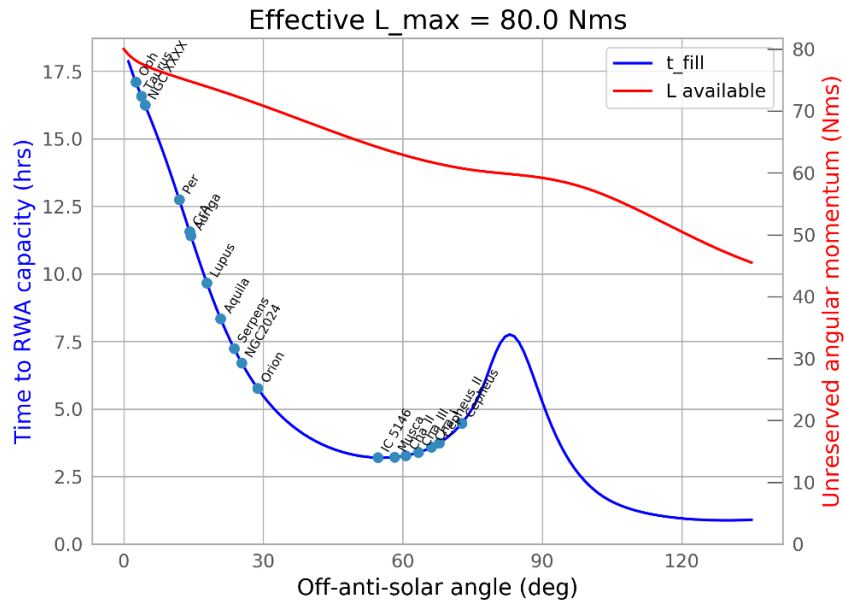


Figure 13. Time required to saturate RWAs for planned targets

The thrusters are used to unload the angular momentum stored in the RWAs. The efficiency of this conversion process is determined by the specific impulse I_{sp} , distance r_{CoM} between the observatory center of mass (CoM), and exhaust angle of the thrusters relative to the CoM-thruster line. The system model assumes observatory parameters consistent with current observatory design, a specific impulse of 150 s consistent with the end-of-life figure from JWST, and a 90 degree angle, i.e. all thrust is converted into angular momentum. The conversion efficiency of propellant mass m into angular momentum L is then given by

$$\frac{dm}{dL} = \frac{1}{r_{CoM} g I_{sp}}$$

independent of the details of the thruster operation.

Given the science target list, a representative target observing sequence was crafted. From this, a yearly distribution of off-anti-solar angles was derived. The SRP torque was integrated over the period of a year weighted by this off-anti-solar angle distribution to produce a total yearly accumulation of angular momentum. With the conversion efficiency above, the system model estimates that OASIS will consume 6.5 kg of propellant over the course of a year to offset the angular momentum accumulation due to solar radiation pressure torque. With an additional 100% contingency and 50% margin, 19.5 kg of propellant is baselined for a 1-year mission.

A number of system optimizations are under consideration that have not been included in the system model here. These include:

Inclusion of a momentum flap – A momentum flap may be included on the spacecraft to move the equilibrium point to a non-zero off-anti-solar angle. If the new equilibrium point is >17 degrees, then observing targets on either side of the equilibrium point will accumulate angular momentum with opposite signs and cancel out, allowing an efficient angular momentum unloading mechanism. If the new equilibrium point is <17 degrees, then the SRP torque will be partially counterbalanced and the total torque on the observatory will be reduced, resulting in longer hold times before unloading and lower total propellant consumption.

Increasing the specular reflectivity of the sunward side of A1 – Photons that are specularly reflected by A1 impart momentum only normal to the reflector surface; the reflected photon carries away the transverse momentum. Photons that are absorbed or diffusely reflected absorb the transverse momentum carried by the incident photon. Therefore by increasing

the specularity of the A1 surface, the transverse F_t term can be significantly reduced. Since this is the dominant term contributing to the SRP torque, the SRP torque may be significantly reduced by making the sunward side of A1 more specularly reflective. This would lead to longer hold times and reduced propellant consumption.

Preferentially aligning RWA wheels with the pitch axis – Since significantly less torque is applied along the other two observatory axes, the RWA wheels may be aligned with the pitch axis. This would increase the total angular momentum capacity along the pitch axis and allow for longer accumulation periods. Alternatively, for a fixed angular momentum capacity it would allow for a smaller cheaper RWA. This has no effect on the propellant consumption.

Preferentially biasing RWA momentum capacity in the positive direction – The symmetric RWA system has equal capability to go to -200 Nms as +200 Nms. If during the unloading process the RWA angular momentum is biased to, for example, +100 Nms, then the RWA has an asymmetric capacity of -300 Nms to 100 Nms. Since the angular momentum management strategy requires the observatory pitch to always be positive, then 300 Nms would be available for use instead of 200 Nms.

2.7 Lifetime

OASIS has two consumables that are needed for the mission: propellant or fuel and inflatant or gas to maintain proper pressure in A1. This begs an obvious and seminal question, “which runs out first, fuel or gas?” This section lends itself to the formulation and analysis of this question and subsequent questions that arise in our discussion.

We denote the mass of the propellant or fuel as m_F and that of the inflatant gas as m_G . This sum is equal to the allowed mass of consumables defined by the launch vehicle capability m_L and the design dry mass m_D , namely

$$m_L = m_D + m_F + m_G. \quad (1)$$

Subtraction of m_D from both sides gives

$$m_L - m_D = m_F + m_G \quad (2)$$

Equation (2) shows that $m_F + m_G$ is fixed. Let us rename $m_L - m_D$ as m_C , the allowed mass of the consumables. Equation (2) becomes

$$m_C = m_F + m_G. \quad (3)$$

At this point in our discussion, two questions arise. The first question is, “how is mission lifetime related to m_C ?” and the second is, “how are m_F and m_G derived?”. As we shall soon see, these questions are not entirely independent.

Consider m_F first. The fuel must be adequate for establishing the science orbit and once achieved, the remainder of the fuel is needed for momentum management and station keeping. The mass of fuel needed to establish orbit, to accommodate the launcher injection, and date of launch dispersions is a fixed quantity denoted m_{F0} . The amount of fuel needed for station keeping (SK) and mission momentum (MM) is proportional to the mission length S . Namely for a mission of length S , the fuel needed for orbit maintenance m_M is

$$m_M = (r_{MM} + r_{SK}) S_F. \quad (4)$$

For the tractability of this analysis, let us call the sum of $r_{MM} + r_{SK}$ the orbit maintenance mass rate, r_M ¹. This enables us to write (4) as

$$m_M = r_M S_F \quad (5)$$

So m_F may be written as

$$m_F = m_{F0} + r_M S_F. \quad (6)$$

We know from other analysis [12] that m_G is given by

¹ Take note that r_{MM} and r_{SK} are not fixed, but evolve with the mission. In the current analysis these values are worst case rates. More sophisticated analysis is in progress.

$$m_G = kS_G^2. \quad (7)$$

We can rewrite (7) in terms of m_F as

$$m_C - m_F = kS_G^2. \quad (8)$$

The mission will end as soon as one of these consumables is exhausted, regardless of if a surplus of the other exists. Therefore, the mission lifetime will be maximized when both consumables have equal lifetimes, namely when

$$S_F = S_G. \quad (9)$$

Substitution of (6) and (8) in (9) gives

$$\frac{m_F - m_{F0}}{r_M} = \sqrt{\frac{m_C - m_F}{k}} \quad (10)$$

Squaring both sides and simplifying gives

$$\frac{1}{r_M^2} m_F^2 - \frac{2m_{F0}}{r_M^2} m_F + \frac{m_{F0}^2}{r_M^2} = \frac{m_C - m_F}{k} \quad (11)$$

Rearrangement of (11) as a standard quadratic equation results in

$$\frac{k}{r_M^2} m_F^2 + \left(1 - \frac{2km_{F0}}{r_M^2}\right) m_F + \left(\frac{km_{F0}}{r_M^2} - m_C\right) = 0. \quad (12)$$

We can immediately solve for m_F using the quadratic formula. Since only positive masses make physical sense, we are guided to choose the positive sign and m_F given as

$$m_F = \frac{r_M^2 \left[\left(\frac{2km_{F0}}{r_M^2} - 1 \right) + \sqrt{1 + \frac{4k}{r_M^2} (m_C - m_{F0})} \right]}{2k}. \quad (13)$$

We can solve for the nominal lifetime by substituting this solution into (6)

$$S_{\max} = \frac{r_M \left[\left(\frac{2km_{F0}}{r_M^2} - 1 \right) + \sqrt{1 + \frac{4k}{r_M^2} (m_C - m_{F0})} \right]}{2k} - \frac{m_{F0}}{r_M}. \quad (14)$$

Figure 14 shows the nominal mission lifetime (designated by a green square) based on the lifetimes of each consumable for a given mass fraction ratio.

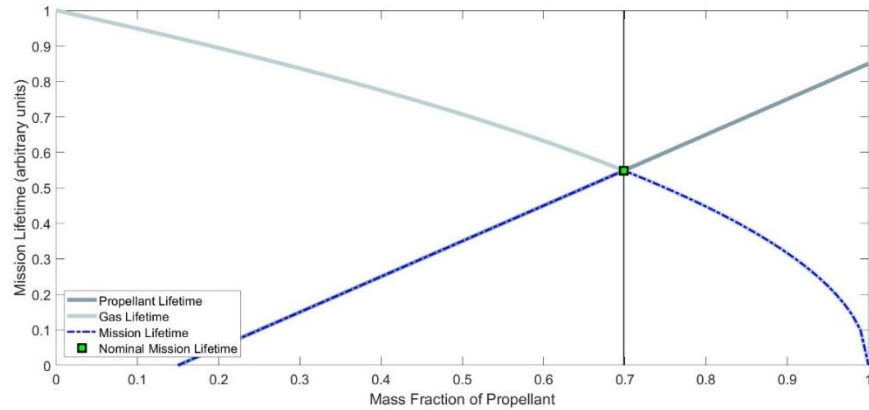


Figure 14. Calculation for the nominal mission lifetime given two consumables. The maximum mission lifetime will occur when the mass fractions of each consumable used result in equal lifetimes.

We now investigate what happens if the rate of each consumable differs from that planned during the actual mission. We generalize the results since the consumption rates of each consumable for OASIS are not yet known. In the following examples, we will assume the actual rates in flight differ by 20%. We first examine the case where the gas is exhausted quicker than planned. In contrast to the above calculation, we cannot determine the mission lifetime by simply substituting in the new gas rate and equating it to the propellant lifetime. This is because we have committed to a particular mass fraction for each consumable and cannot adjust this post launch (i.e. we are stuck on the black vertical line shown in Figure 14). Therefore, the actual mission lifetime will be dictated by the new gas lifetime function at the mass fraction specified in the architecture, which will not be the optimum lifetime. This scenario is displayed visually in Figure 15. Similarly, if rather, the propellant is expelled quicker than planned, then the new mission lifetime will be on the new propellant lifetime function at the mass fraction specified, shown in Figure 16. This demonstrates that if the uncertainty in the consumption rates are large, the actual mission lifetime could be much shorter than that planned. We note that the mission lifetime is not extended in the opposite case where one consumption rate is lower than planned. This is because the mission lifetime is still constrained by the lifetime of the other consumable. An extended mission life would only occur in the event that both rates are lower than expected.

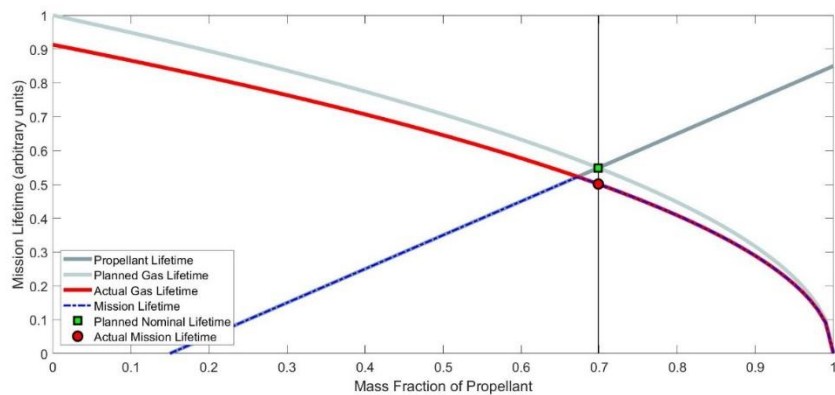


Figure 15. Difference in mission lifetime if the gas is consumed faster than expected. The updated mission lifetime is now determined by the gas lifetime function at the mass fraction allocation.

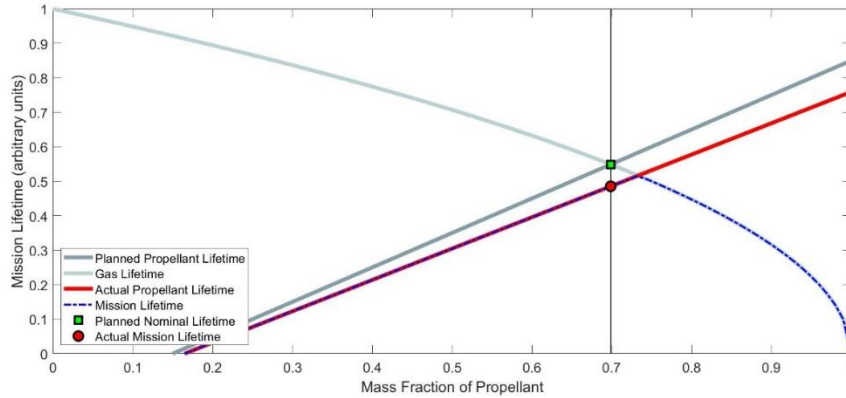


Figure 16. Difference in mission lifetime if the propellant is consumed faster than expected. The updated mission lifetime is now determined by the propellant lifetime function at the mass fraction allocation.

Now that we conceptually understand how the mission lifetime will vary with uncertainty, we expand our analysis to determine which mass allocation the lifetime is most sensitive to. To do this, we determine how the mission lifetime will change if we have an error in our prediction values of k , r_M , or m_{F0} from (6) and (7). We adjust the prediction error of each value up to 200% while holding all other variables, m_F , and m_G constant.

The planned mass allocation is such that each consumable has a lifetime of 1 year. Inputs into (6) and (7) are based on preliminary analysis which we set to: $r_m=34.2$ kg/yr, $m_{F0}=97.5$ kg, $m_F=131.7$ kg, $m_G=250$ kg, $k=250$ kg/yr², and $m_C=381.7$ kg. We note that these are rough estimates and should be considered for demonstration purposes only—more analysis is needed to determine official values. However, the exact reference values used will not change the overall trends. Figure 17 shows the resulting mission lifetime for a given error. It is clear that the mission lifetime is most sensitive to m_{F0} , followed by r_M , and k . This makes sense upon inspection of (6) and (7): the lifetime is proportional to these variables by $S \propto \frac{1}{\sqrt{k}}$, $S \propto \frac{1}{r_m}$, and $S \propto -m_{F0}$. Therefore, deviations in m_{F0} create the quickest changes in mission lifetime. For the planned values considered, Figure 17 indicates that if the actual value of m_{F0} is greater than 17.5% its planned value, the length of the mission will be shorter than the threshold mission. Although the lifetime has the highest sensitivity to m_{F0} , it is the term that in practice, has the lowest uncertainty. On the other hand, the term with the lowest sensitivity, k , has the largest uncertainty associated with its estimated value. An important implication of Figure 17 is that if we can lower the mass necessary for m_{F0} , we can extend the mission lifetime by re-allocating the mass to momentum maintenance and gas usage.

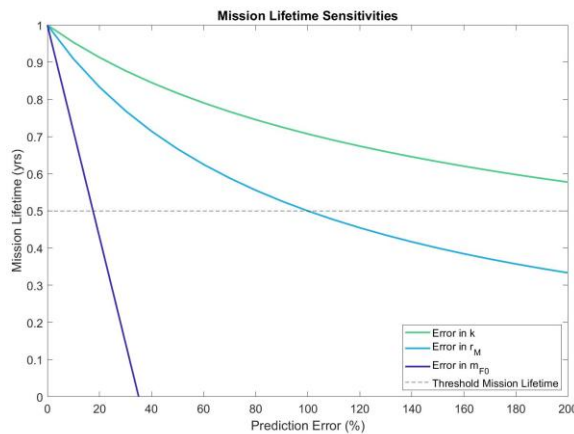


Figure 17. Mission lifetime sensitivity to errors in planned consumable usage. The lifetime is most sensitive to deviations of m_{F0} from its planned value

In order to determine the impact on the lifetime, we must have estimates of the variances of the parameters, as the impact is the product of the sensitivity and uncertainty (square root of variance). Consider Figure 18, line A is a 10% uncertainty in values of the orbital parameters, which is selected as a discussion point, at this level of uncertainty, at 10% change in m_{F0} costs 30% in lifetime as shown by line B. The uncertainty in the determination of the gas mass depends on our knowledge of the impact of the micrometeoroids and the environment. Our work in this area indicate that both factors have large uncertainties and so a predicted gas mass may be significantly greater than 100% (to the right of Line C). [12] This is what is motivating our planned experiments to improve the fidelity of our predictions and hopefully reduce the area lost. This very naïve analysis shows the criticality to OASIS of understanding our predictions for consumable usage and the uncertainties in those rates.

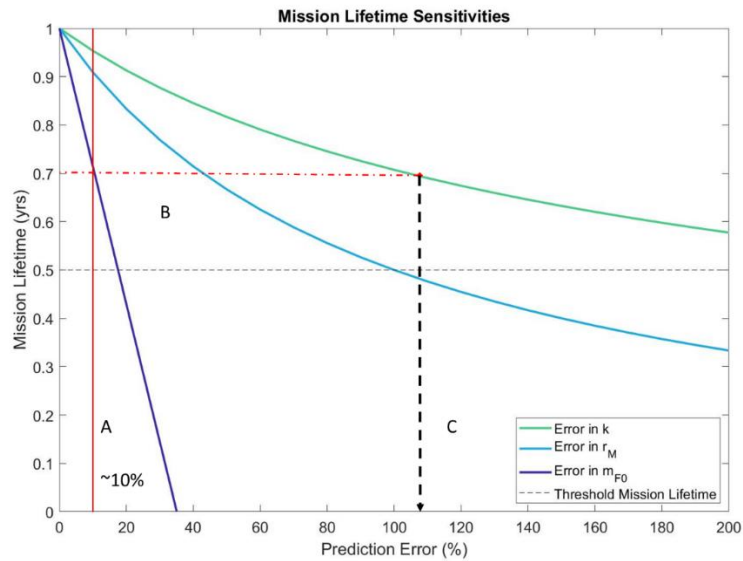


Figure 18. Estimate of impact on lifetime from uncertainty in parameter values. Line A represents a 10% uncertainty in m_{F0} , which corresponds to a reduction of the mission lifetime of 30% (Line B). Prediction errors of >100% in the other two variables will have similar impacts on the mission lifetime (Line C).

2.8 Thermal

A thermal model of A1 was developed for the purposes of calculating temperatures throughout the reflector. The properties of the transparent canopy and the reflective layer are shown in Figure 19. The canopy layer is a solar-opaque black Kapton 275XC, and the reflective surface on the reflector is vapor deposited aluminum (VDA) and the external side is modeled as silicon-coated Kapton, with the same thermo-optical properties as the James Webb Space Telescope sunshield. The internal pressure is modeled at 3.5 Pa.

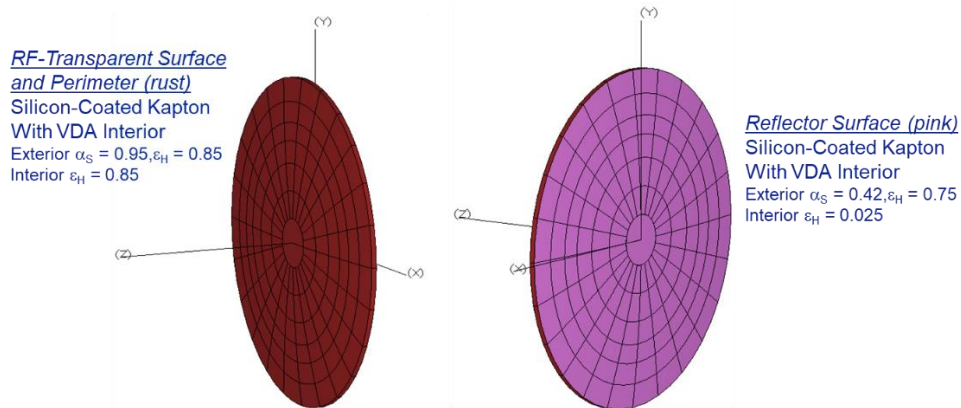


Figure 19. Thermo-optical properties used in the OASIS thermal model.

The predicted temperatures are given in Figure 20; for all panels the left side of the x-axis represents the sun angle with the observatory looking anti-sunward, and the right most axis is 45 degrees from the sun line. In panels (a) and (b), the hottest node is given by the orange trace, the mean nodal temperature is the gray or middle trace, and the coldest node is given by the blue trace. The left panel (a) shows the temperatures of the reflector. For panels (a) and (b), the spacing between the orange and blue traces is a measure of the temperature diversity of the surface, and surrogate for thermally induced (low frequency) distortion. This distortion is highest when A1 is edge on with the sun. Panel (c) is the mean temperature of the front and back panels and is our estimate of the gas temperature, which for the most likely pointing angles is about 235K.

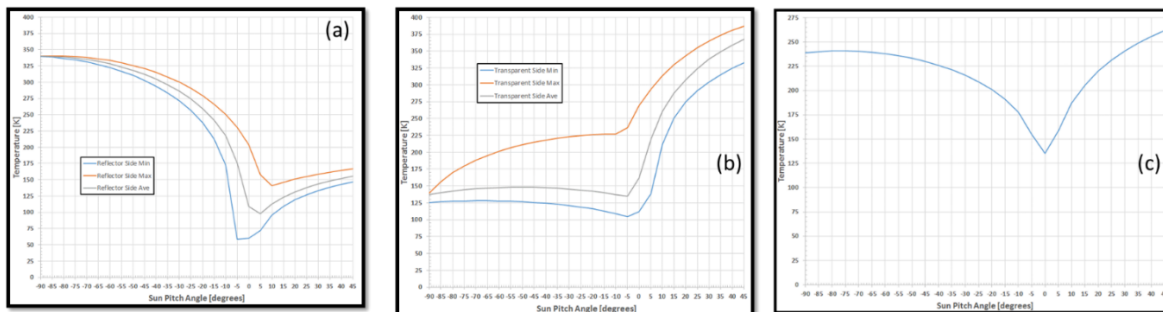


Figure 20. Temperatures predicted by the OASIS thermal model, panel (a) reflector temperatures, panel (b) canopy temperatures, panel (c) estimated gas temperatures.

It is worth noting that the model predicts negligible thermal conduction in either the membranes or due to the fill gas. This means that the membrane temperature is largely a function of insolation and sun-angle geometry.

2.9 Testing

Modeling plays a central role in the development of OASIS and the validation of those models is key to the success of the mission. To validate some of the key modeling assumptions and results, several test campaigns have been planned and have been started at the time of this writing, but are not complete.

Vacuum testing at Northrop Grumman was conducted in July 2021. A 1 m diameter (Hencky) reflector was inflated with various fill gasses; helium, argon and xenon. The surface shape was measured via deflectometry in both ambient and vacuum conditions to provide data for calibration and validation of finite element modeling [14]. Additionally, a solar simulator was used to drive a thermal gradient and provide additional distortion cases to allow the FEM to be anchored to test data. Finally, the inflatable was mechanically punctured to demonstrate that a mechanically rough hole does not create

a propagating tear and demonstrate that when A1 is reinflated via pressure control, the original shape is reestablished. Additional testing is planned at atmospheric pressure at the University of Arizona with a 1 m parabolic reflector now under construction at L'Garde.

Hypervelocity (micrometeoroid) testing is also scheduled for August 2021, and is not complete at the time of this writing. It is expected that this testing will allow for a more precise determination of the area lost to micrometeoroid collisions.

3. SUMMARY AND NEXT STEPS

We have presented a MidEX mission concept for an inflatable telescope stationed at the L1 Lagrange point. The architecture proposed would enable a large collecting area at a fraction of the cost and mass budgets compared to traditional space telescopes. The A1 reflector will be approximately 20 m in diameter with a radius of curvature of 50 m. The observing strategy will require A1 to generally point between 17-60 degrees off the anti-solar direction, with the Earth and Moon within this field of view for the majority of the mission. Torque due to solar radiation pressure will be managed using reaction wheels and thrusters. We also addressed the optimization of the mission lifetime for our two consumables; propellant and gas. We demonstrated how we will model and verify by test thermal distortions on A1. Next steps include testing of small-scale inflatables to inform understanding of the effects of fill gas and micrometeoroid punctures.

REFERENCES

- [1] Christopher Walker et al., "Orbiting Astronomical Satellite for Investigating Stellar Systems (OASIS) Following the Water Trail from the Interstellar Medium to Oceans," SPIE Paper #11820-26, this proceeding, 2021.
- [2] Project Echo, URL <https://www.nasa.gov/centers/langley/about/project-echo.html>, last accessed 13 July 2021
- [3] Hans H. Kretschmer "A Camera Platform in Space," Optical Engineering 1(4), 104117 (1 May 1963). <https://doi.org/10.1117/12.7971246>
- [4] B. Authier and L. Hill "Large Inflatable Parabolic Reflectors In Space", Proc. SPIE 0598, Instrumentation for Submillimeter Spectroscopy, (21 April 1986); <https://doi.org/10.1117/12.952331>
- [5] Mingwan Soh, Jun Ho Lee, and Sung-Kie Youn "An inflatable circular membrane mirror for space telescopes", Proc. SPIE 5638, Optical Design and Testing II, (10 February 2005); <https://doi.org/10.1117/12.571628>
- [6] Ivan Bekey "Very large yet extremely lightweight space imaging systems", Proc. SPIE 4849, Highly Innovative Space Telescope Concepts, (18 December 2002); <https://doi.org/10.1117/12.460755>
- [7] James D. Moore, Brian G. Patrick, Surya Chodimella, Dan Marker, and Brett deBlonk "Design and testing of a one-meter membrane mirror with active boundary control", Proc. SPIE 5899, UV/Optical/IR Space Telescopes: Innovative Technologies and Concepts II, 58990Z (18 August 2005); <https://doi.org/10.1117/12.618547>
- [8] Gerard Theodore van Belle, Aden Baker Meinel, and Marjorie Pettit Meinel "The scaling relationship between telescope cost and aperture size for very large telescopes", Proc. SPIE 5489, Ground-based Telescopes, (28 September 2004); <https://doi.org/10.1117/12.552181>
- [9] Aden B. Meinel and Marjorie P. Meinel "Inflatable membrane mirrors for optical passband imagery," Optical Engineering 39(2), (1 February 2000). <https://doi.org/10.1117/1.602393>
- [10] R.E. Freeland, G.D. Bilyeu, G.R. Veal, M.D. Steiner, D.E. Carson, "Large inflatable deployable antenna flight experiment results", Acta Astronautica, Volume 41, Issues 4-10, 1997, Pages 267-277
- [11] Siddhartha Sirsi et al., "Parametric design study of all reflective 20m telescope with an inflatable primary antenna for Orbiting Astronomical Satellite for Investigating Stellar Systems (OASIS)," SPIE Paper #11820-28, this proceeding, 2021.
- [12] Jonathan Arenberg et al., "Environmental Impacts on OASIS's Pressure Control," SPIE Paper #11820-31, this proceeding, 2021.
- [13] Yuzuru Takashima et al., "All reflective THz telescope design with a 20m inflatable primary antenna for Orbiting Astronomical Satellite for Investigating Stellar Systems (OASIS) mission," SPIE Paper #11820-27, this proceeding, 2021.
- [14] Arthur Palisoc, et al, SPIE Paper #11820-XX, this proceeding, 2021
- [15] Quach et al, "Deflectometry-Based Thermal Vacuum Testing for a Pneumatic Terahertz Antenna", SPIE Paper #11820-XX, this proceeding, 2021
- [16] Jeffrey S. Parker, and Rodney L. Anderson, "Low-Energy Lunar Trajectory Design", Wiley, 2014.